ARTICLE TEMPLATE

Ordered structures formed by ultrasoft, aspherical particles

Markus Weißenhofer[a], Davide Pini[b], and Gerhard Kahl[a]

[a]Institut für Theoretische Physik and Center for Computational Materials Science (CMS), TU Wien, Wiedner Hauptstraße 8-10, A-1040 Wien, Austria; [b]Dipartimento di Fisica "A. Pontremoli", Università degli Studi di Milano, Via Celoria 16, I-20133 Milano, Italy

ARTICLE HISTORY
Compiled July 3, 2018

ABSTRACT
We have applied the formalism of classical density functional theory to study the shape and the orientation of the density profiles $\rho(\mathbf{r})$ formed by aspherical, ultrasoft particles. For simplicity we have considered particles with an elliptic shape, characterized by an aspect ratio λ. The $\rho(\mathbf{r})$'s are obtained via the minimization of the grand-potential functional $\Omega[\rho]$, for which we have used a mean-field format. The optimization of $\Omega[\rho]$ is numerically realized in a free (i.e., unbiased) manner minimizing the functional with respect to the density profile, which we have discretized in the unit cell of the lattice on 80^3 grid points. Keeping the temperature fixed and varying the chemical potential and λ, we have investigated the impact of these parameters on the density profile.

KEYWORDS

1. Introduction

It has by now become common knowledge that anisotropy is a relevant driving force in establishing and triggering self-assembly of colloidal particles.

In the past decade, the effect of particle shape on the symmetry of high-density phases has been studied in considerable detail, especially in hard ellipsoids [1] and hard polyhedra where a range of liquid-crystalline, quasicrystalline, plastic-crystalline, and crystalline structures were reported. [2–6]. Besides being related to particle shape, anisotropy can also be introduced via the effective interactions as in the case of patchy particles, i.e., hard, spherical particles with an additional interaction which is localized at specific domains on the particle surface [7–10].

In order to grasp as faithfully as possible the impact of anisotropy on the properties of the system, considerable effort has been dedicated during the past years to simulation-based (for an overview see [11, 12]) and theoretical methods: including anisotropy in these frameworks represents a major challenge; this holds in particular in the case of theory, where it is both conceptually and numerically very difficult to account for it on a quantitative level.

Classical density functional theory (DFT) ranges undoubtedly among the most fruitful and powerful concepts that have been and are still used to describe the structural

CONTACT G. Kahl. Email: gerhard.kahl@tuwien.ac.at

and thermodynamic properties of (soft) condensed-matter systems [13–15]. In this contribution we demonstrate that DFT allows to calculate non-trivial single particle density profiles $\rho(\mathbf{r})$, as they obviously arise in ordered structures formed by aspherical particles.

So far, in DFT calculations (based on some reliable format for the grand-potential energy functional $\Omega[\rho]$) an educated guess for $\rho(\mathbf{r})$ was assumed, i.e., some function which was expected to represent the density profile and which was characterized by a few parameters. Minimization of the *functional* $\Omega[\rho]$, which thus has become a *function* of these parameters, was then obtained by minimizing the function with respect to the parameters. In a recent contribution by Pini *et al.* [16] it was shown that present day computational power in combination with highly efficient and reliable numerical optimization techniques enable to perform the minimization of Ω with respect to $\rho(\mathbf{r})$ in an *unbiased* manner. This could be achieved by representing $\rho(\mathbf{r})$ in a finite volume (e.g., in a lattice cell), discretized on a sufficiently fine grid (with typically 80^3 to 100^3, or even more, grid points) in r-space, avoiding thereby an *a priori* bias on the shape of the density profile. Minimization is then performed by varying the values of $\rho(\mathbf{r})$ on the grid points and – if required – by optimizing the shape of the lattice cell. In [16], the authors have shown with this approach that even a spherically symmetric two-body interaction may lead to quite complex structures, which would have likely escaped a biased search. The broad applicability of this method was demonstrated in subsequent work by Roth and coworkers [17–19] and again by Pini and Parola [20].

This has motivated us to turn to the density profile of particles that are aspherical in their shape and/or their interaction. In our investigations we have focused on ultrasoft (i.e., penetrable), aspherical particles. During the past decade, (colloidal) particles that interact via ultrasoft potentials have often been viewed as "effective particles", representing considerably more complex macromolecules with an intricate internal structure, consisting of hundreds or thousands of atomistic entities. Examples for such ultrasoft "effective particles", which have been discussed in literature are polymers [21] or dendrimers [22]. As will be detailed in the body of the manuscript, some of these ultrasoft particles are able to form particular mesophases, termed in literature "cluster crystals" [23]. In general these "effective particles" are assumed – mostly for simplicity – to be spherically symmetric, leading to a simple dependence of their interactions on the distance. However, as has been evidenced in more detailed investigations on isolated dendrimers or ensembles of dendrimers, these macromolecules are definitely aspherical; their shape can actually be more appropriately represented by an ellipsoid of revolution, whose semi-axes are determined by diagonalizing their radius of gyration tensor [24–26].

We have then assumed for their effective interaction a generalization of the spherically symmetric generalized exponential model potential [23, 27], introducing in a Gay-Berne-type fashion [28, 29] anisotropy via the characteristic length scale of the potential: the interaction between two particles now depends on the center-to-center vector between the particles and the respective orientations of the particles in space. Via the assumed functional form of the potential, the particles are elliptic in their shape and are characterized by their aspect ratio λ, i.e., the ratio of the values of their principal axes. In an effort to reduce complexity, we have assumed that the orientations of the particles on the lattice sites of the underlying lattice are parallel. For the excess part of the energy functional we have opted for a mean-field format, justified by the fact that we consider ultrasoft (i.e., penetrable) particles [30]. In our numerical approach *both* the lattice of the ordered equilibrium structure (expressed via the three lattice vectors $\mathbf{a}_i$, $i = 1, 2, 3$) and the single-particle density profile have been obtained

for a given temperature and chemical potential via a free, i.e., unbiased optimization of the functional $\Omega[\rho]$ with respect to $\rho(\mathbf{r})$. By changing the temperature, the chemical potential (or, equivalently, the density) and the aspect ratio λ, we have investigated the impact of these quantities on the shape and on the orientation of the density profile.

The manuscript is arranged as follows: in the subsequent section we briefly present our model and the underlying interaction, we summarize the relevant aspects of the DFT formalism and provide details about our numerical implementation, and finally describe the tools that allow us to analyze and to characterize the emerging single-particle density profiles. In Section 3 we present and discuss the results; the contribution is closed with our concluding remarks.

2. Model and methods

2.1. The model

In this contribution we have assumed that the particles interact via an aspherical, ultrasoft potential, which can be viewed as a generalization of the (spherically symmetric) generalized exponential potential of index n (GEM-n) [23, 27, 31, 32] which is given by

$$\Phi(r) = \varepsilon \exp[-(r/\sigma)^n]; \tag{1}$$

here ε and σ are energy and length scales, respectively. If the index n is larger than two, this interaction has been shown to belong to the so-called $Q^{\pm}$ class, i.e., a set of potentials for which the formation of stable clusters of overlapping particles has been predicted [23, 27, 30–33]; this particular feature can be traced back to the fact that there exists a non-vanishing k-vector for which the Fourier transform of the potential, $\tilde{\Phi}(k)$, attains a negative minimum. In the following (and in order to establish connections to the above mentioned previous studies) we have fixed $n = 4$, both for the spherical and the aspherical case.

Asphericity of the interaction can be introduced – extending original ideas of Gay and Berne [28] – via ε and σ, which are now assumed to depend on the vector $\mathbf{r}$ between the centers of the particles and on their respective orientations in space (i.e., $\mathbf{u}$ and $\mathbf{u}'$ with respect to some arbitrary coordinate system – see left panel of Fig. 1). Thus our potential, $\Phi(\mathbf{r}; \mathbf{u}, \mathbf{u}')$ is given by

$$\Phi(\mathbf{r}; \mathbf{u}, \mathbf{u}') = \varepsilon(\mathbf{r}; \mathbf{u}, \mathbf{u}') \exp\left[-\left(\frac{r}{\sigma(\mathbf{r}; \mathbf{u}, \mathbf{u}')}\right)^n\right]. \tag{2}$$

Ever since the work of Gay and Berne [28], different choices for the dependence of σ and ε on $\mathbf{r}$, $\mathbf{u}$ and $\mathbf{u}'$ have been proposed in literature. In this contribution we have opted for the following functional form of $\sigma(\mathbf{r}; \mathbf{u}, \mathbf{u}')$, which was proposed by Ghoufi *et al.* [29] for particles modelled as ellipsoids of revolution with longitudinal and transverse axes of length respectively $\sigma_{\parallel}$, $\sigma_{\perp}$ (see Fig. 2).

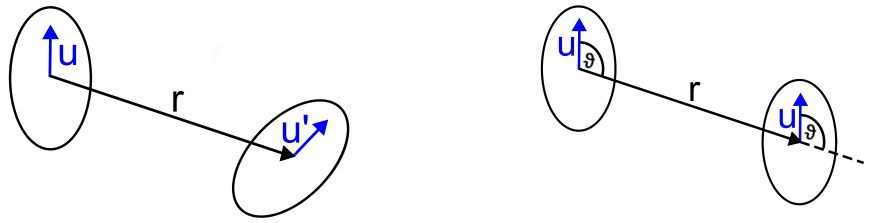

Figure 1. (color online) Left panel: schematic sketch of two interacting aspherical particles; $\mathbf{u}$ and $\mathbf{u}'$ denote the respective orientational unit vectors of the particles, while $\mathbf{r}$ is the center-to-center vector. Right panel: schematic sketch of two *parallel* interacting spherical particles, as they are studied in this contribution (see Equation (4) for the corresponding potential, the angle ϑ is defined in Equation (6); same notation as in the left panel).

$$\sigma(\mathbf{r};\mathbf{u},\mathbf{u}') = \sigma_0 \left(1 - \frac{\chi}{r^2}\frac{(\mathbf{r}\cdot\mathbf{u})^2 + (\mathbf{r}\cdot\mathbf{u}')^2 - 2\chi(\mathbf{r}\cdot\mathbf{u})(\mathbf{r}\cdot\mathbf{u}')(\mathbf{u}\cdot\mathbf{u}')}{1-\chi^2(\mathbf{u}\cdot\mathbf{u}')^2}\right)^{-1/2} , \quad (3)$$

where σ_0 sets the unit length. In the above expression we have introduced the anisotropy parameter $\chi = (\lambda^2-1)/(\lambda^2+1)$, where λ is the aspect ratio $\lambda = \sigma_\parallel/\sigma_\perp$. In this paper we shall consider prolate ellipsoids such that $\lambda > 1$. For simplicity (and unlike Ghoufi *et al.* [29]) the energy scale parameter ε is assumed to be constant, i.e., $\varepsilon(\mathbf{r};\mathbf{u},\mathbf{u}') \equiv \varepsilon$.

In our investigations the orientational unit vectors of two particles, $\mathbf{u}$ and $\mathbf{u}'$, that populate two different lattice positions, are assumed to be parallel: since their direction in space is arbitrary, but is kept fixed throughout the calculations, we can set $\mathbf{u} = \mathbf{u}' = \mathbf{n}$ (with $|\mathbf{n}| = 1$); we thus arrive at the following expression for $\Phi(\mathbf{r};\mathbf{u},\mathbf{u}') = \Phi(\mathbf{r})$:

$$\Phi(\mathbf{r}) = \varepsilon \exp\left[-\left(\frac{r}{\sigma(\mathbf{r})}\right)^4\right] , \quad (4)$$

with

$$\sigma(\mathbf{r}) = \frac{\sigma_0}{\sqrt{1+(\lambda^{-2}-1)\left(\frac{\mathbf{r}\cdot\mathbf{n}}{r}\right)^2}} = \frac{\sigma_0}{\sqrt{1+(\lambda^{-2}-1)\cos^2\vartheta}} , \quad (5)$$

where

$$\frac{\mathbf{r}\cdot\mathbf{n}}{r} = \cos\vartheta; \quad (6)$$

the angle ϑ is enclosed by the vectors $\mathbf{r}$ and $\mathbf{n}$ (see right panel of Fig. 1). Thus $\Phi(\mathbf{r})$ can alternatively be written as $\Phi(r,\vartheta)$. According to Equations (5), (6), the isosurfaces of $\Phi(r,\vartheta)$ are ellipsoids with their longitudinal axis parallel to $\mathbf{n}$. A few examples for the r- and ϑ-dependence of $\Phi(r,\vartheta)$ are shown in the panels of Fig. 3, keeping either of the

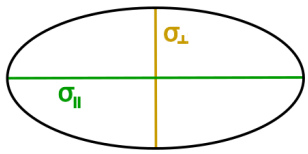

Figure 2. Schematic view of an aspherical particle with ellipsoidal shape as it is used in this contribution: the parameters $\sigma_\parallel$ and $\sigma_\perp$ define via $\lambda = \sigma_\parallel/\sigma_\perp$ the aspect ratio λ. The particle is an ellipsoid of revolution around $\sigma_\parallel$.

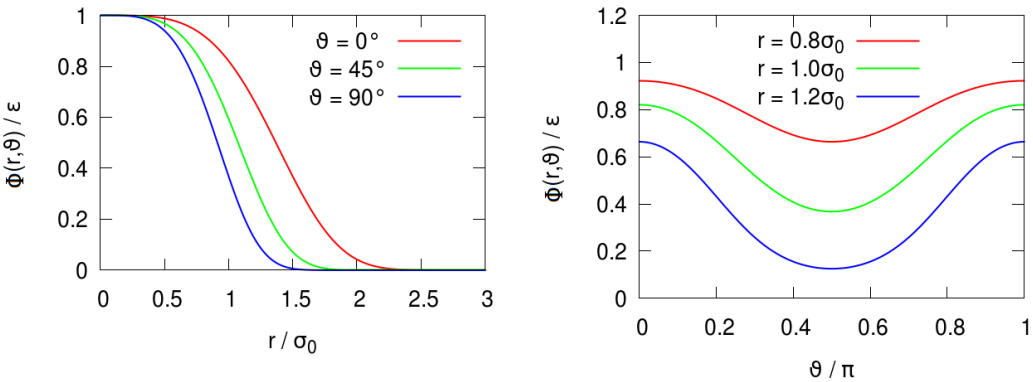

Figure 3. (color online) Left panel: $\Phi(r, \vartheta)$ as defined in Equations (4) and (5) as a function of r for selected values of ϑ (as labeled). Right panel: $\Phi(r, \vartheta)$ as a function of ϑ for selected values of r (as labeled). For this particular case $\lambda = 1.5$.

two arguments fixed (there λ is assumed to be 1.5). Note that similar models – albeit with an exponent $n = 2$ (i.e., Gaussian potentials) – have been used in Refs. [34, 35].

In a similar manner, the Fourier transform of the potential $\tilde{\Phi}(\mathbf{k})$, can be written as $\tilde{\Phi}(k, \phi)$ where $k = |\mathbf{k}|$ and ϕ is now the angle enclosed by $\mathbf{k}$ and the preferred axis in k-space (see Fig. 4). It is readily shown that the isosurfaces of $\tilde{\Phi}(k, \phi)$ are also ellipsoids. Specifically, one has

$$\tilde{\Phi}(k, \phi) = \varepsilon \sigma_\parallel \sigma_\perp^2 \Psi\Big(\sigma_0 k \sqrt{1 + (\lambda^2 - 1)\cos^2\phi}\Big) \quad , \tag{7}$$

where the function Ψ is *the same* as that obtained for spherical particles by performing the Fourier transform of Equation (1). Therefore, also in the case of asphericity, $\tilde{\Phi}(\mathbf{k})$ shows for $n > 2$ negative Fourier components; however, in contrast to the spherical case, the positions of the minima of $\tilde{\Phi}(\mathbf{k})$ show for $\lambda > 1$ an additional angular dependence. While in the spherically symmetric case the locus where $\tilde{\Phi}(\mathbf{k})$ takes its minimum is obviously the surface of a sphere, in the aspherical case we are dealing with it is an ellipsoid.

2.2. Classical density functional theory

Working in the grand-canonical ensemble (i.e., at given temperature T, volume V, and chemical potential μ), the central quantities of classical density functional theory (DFT) [13, 14] are the single-particle density profile

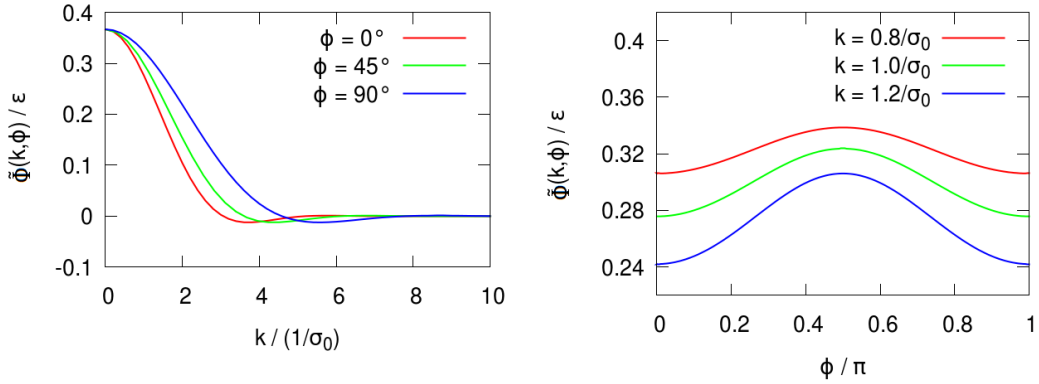

Figure 4. (color online) Left panel: $\tilde{\Phi}(k,\phi)$ as defined in Equation (16) as a function of k for selected values of ϕ (as labeled). Right panel: $\tilde{\Phi}(k,\phi)$ as a function of ϕ for selected values of k (as labeled). For this particular case $\lambda = 1.5$.

$$\rho(\mathbf{r}) = \left\langle \sum_i \delta(\mathbf{r} - \mathbf{r}_i) \right\rangle \tag{8}$$

and the grand-potential functional $\Omega[\rho]$, given (in the absence of an external potential) by

$$\beta\Omega[\rho] = \beta\mathcal{F}_{\rm id}[\rho] + \beta\mathcal{F}_{\rm ex}[\rho] - \beta\mu \int_V d\mathbf{r}\rho(\mathbf{r}); \tag{9}$$

in the above equations the $\mathbf{r}_i$ are the positions of the particles, $\beta = 1/(k_{\rm B}T)$, $k_{\rm B}$ being the Boltzmann constant, and $\langle \dots \rangle$ denotes the grand-canonical ensemble average.

$\mathcal{F}_{\rm id}[\rho]$ and $\mathcal{F}_{\rm ex}[\rho]$ are, respectively, the ideal and excess parts of the Helmholtz free energy functionals, the former one being given by

$$\mathcal{F}_{\rm id}[\rho] = k_{\rm B}T \int_V d\mathbf{r}\rho(\mathbf{r}) \left\{ \ln\left[\Lambda^3\rho(\mathbf{r})\right] - 1 \right\}; \tag{10}$$

Λ is the thermal wavelength. As we are dealing with ultrasoft potentials, we can assume – as laid out in [30] – a mean-field format for the excess part of the free energy functional, namely,

$$\mathcal{F}_{\rm ex}[\rho] = \frac{1}{2} \int\int d\mathbf{r}d\mathbf{r}'\rho(\mathbf{r})\Phi(\mathbf{r} - \mathbf{r}')\rho(\mathbf{r}'). \tag{11}$$

The equilibrium single-particle distribution is obtained by minimizing $\Omega[\rho]$ with respect to $\rho(\mathbf{r})$, i.e., by solving

$$\frac{\delta\Omega[\rho]}{\delta\rho(\mathbf{r})} = 0. \tag{12}$$

As we are looking for the equilibrium density profile of ordered phases, we can assume that $\rho(\mathbf{r})$ is periodic with respect to an underlying lattice (specified by lattice vectors $\mathbf{a}_1$, $\mathbf{a}_2$, and $\mathbf{a}_3$), i.e.,

$$\rho(\mathbf{r}) = \rho(\mathbf{r} + \mathbf{a}_i) \qquad i = 1, 2, 3. \tag{13}$$

The corresponding reciprocal lattice vectors are denoted by $\mathbf{b}_i$, $i = 1$, 2, 3. The liquid (i.e., disordered) case is covered in this formalism by setting $\rho(\mathbf{r}) \equiv$ const. In this case, Equations (10) and (11) give the free energy of the compressibility route of the random-phase approximation [36], i.e., the familiar van der Waals expression.

Due to its periodicity, $\rho(\mathbf{r})$ can be expressed as a Fourier series over the reciprocal lattice vectors, i.e.,

$$\rho(\mathbf{r}) = \sum_{\mathbf{m}} \exp\left[-i\mathbf{k}_{\mathbf{m}} \cdot \mathbf{r}\right] \hat{\rho}_{\mathbf{m}} \qquad \text{with} \qquad \hat{\rho}_{\mathbf{m}} = \frac{1}{v} \int_{\mathcal{C}} d\mathbf{r} \exp\left[i\mathbf{k}_{\mathbf{m}} \cdot \mathbf{r}\right] \rho(\mathbf{r}) \tag{14}$$

where $\mathcal{C}$ is the unit cell with volume v and with

$$\mathbf{k}_{\mathbf{m}} = \sum_{i=1}^{3} m_i \mathbf{b}_i \qquad \mathbf{m} = (m_1, m_2, m_3) \qquad m_i = 0, \pm 1, \pm 2, \ldots \quad . \tag{15}$$

Further we introduce the Fourier-transform of the (non-periodic) potential

$$\tilde{\Phi}(\mathbf{k}) = \int_V d\mathbf{r} \exp\left[-i\mathbf{k} \cdot \mathbf{r}\right] \Phi(\mathbf{r}). \tag{16}$$

When solving Equation (12) numerically in practical applications of DFT, simple, parametrized functions have been used during the past years as an ansatz (or educated guess) for the density profile, whose parameters were chosen such that $\Omega[\rho]$ is minimized for a given lattice structure; comparing the ensuing results for a preselected set of candidate structures have led to the final result.

In the present contribution, on the other hand, we shall resort to an unbiased optimization along the lines laid out in [16–20]. To this end, in our numerical implementation of the DFT formalism $\rho(\mathbf{r})$ has been discretized on N^3 grid points of the unit cell $\mathcal{C}$, i.e.,

$$\rho(\mathbf{r}) \to \rho_{\mathbf{n}} \tag{17}$$

where $\mathbf{n}$ stands for the N^3 values of $\rho(\mathbf{r})$ on this grid. Furthermore, we introduce the nine Cartesian components of the lattice vectors $\mathbf{a}_i$ (or, equivalently, of the $\mathbf{b}_i$) as additional parameters to be optimized in solving Equation (12). We remark that here, at variance with [16, 20], the lattice vectors are *not* assumed to be mutually orthogonal.

As discussed in [16], optimization with respect to the lattice vectors is of paramount importance in order to prevent the occurrence of local minima of the grand-potential

functional such as defective configurations, which would otherwise be those most frequently observed as a consequence of the intrinsic periodicity of the density profile being incommensurate with the size of the box where it is sampled. Nevertheless, the regular structures obtained by this procedure are still local minima of the grand potential Ω, and there is no guarantee that the outcome of a specific optimization run coincides with the absolute minimum of Ω for the thermodynamic state at hand. This uncertainty is, we fear, intrinsic to the problem, and there is little one can do about it, except for trying to reduce it by sampling the free-energy landscape as thoroughly as possible, e.g. by starting the minimization from different trial density profiles.

Once the discretization – see Equation (17) – has been performed, the functional $\Omega[\rho]$ becomes a *function* Ω of the N^3 variables $\rho_{\mathbf{n}}$ and of the nine variables specifying the components of the $\mathbf{a}_i$ (or $\mathbf{b}_i$), i.e.,

$$\Omega[\rho] \to \Omega(\rho_{\mathbf{n}}, \mathbf{a}_i) = \Omega(\rho_{\mathbf{n}}, \mathbf{b}_i). \tag{18}$$

$\Omega(\rho_{\mathbf{n}}, \mathbf{b}_i)$ can be written after some algebra as

$$\frac{\beta}{V}\Omega(\rho_{\mathbf{n}}, \mathbf{b}_i) = \frac{1}{N^3}\sum_{\mathbf{n}} \rho_{\mathbf{n}} \left[\ln(\Lambda^3\rho_{\mathbf{n}}) - 1 - \beta\mu\right] + \frac{\beta}{2N^6}\sum_{\mathbf{m}} \hat{\rho}_{\mathbf{m}}\tilde{\Phi}(\mathbf{k}_{\mathrm{m}})\hat{\rho}_{-\mathbf{m}}. \tag{19}$$

In this expression, the first sum is extended over the N^3 grid points in the unit cell (and thus in r-space), while the second sum extends over N^3 points in reciprocal space.

In the following we specify (and justify) the numerical parameters that we have used: detailed numerical tests have shown that for the potential at hand and for the considered parameter range (i.e., temperature, chemical potential, density, etc.) $N = 80$ guaranteed a sufficient numerical accuracy (leading to a relative accuracy of Ω of 10^{-8} to 10^{-9}). For the numerical Fourier transform of the potential $\Phi(\mathbf{r})$ we have used a standard Fast Fourier Transform algorithm [37], where $\tilde{\Phi}(\mathbf{k})$ was discretized on 80^3 grid points. The grid size was chosen in such a way that $\Phi(r) < 10^{-15}$ at the r-value where the Fourier integral was truncated. Moreover, in order to keep the computational cost low, the sum over $\mathbf{m}$ in Equation (19) was truncated at some appropriately chosen upper limit for the m_i. In an effort to fully grasp the asphericity in the potential, we carefully checked the truncation in reciprocal space: as the results for $\beta\Omega\sigma_0^3/V$ obtained for selected cases for truncation at $|m_i| = 5$ differed by less than 10^{-9} from the data obtained at $|m_i| = 7$, we opted for the former choice.

As a stringent test for the numerical accuracy we have considered Poisson sum rule, i.e.

$$v\sum_{\mathbf{n}} \Phi(n_i, \mathbf{a}_i) = \sum_{\mathbf{m}} \tilde{\Phi}(m_i, \mathbf{b}_i), \tag{20}$$

which we found to be fulfilled with a relative numerical accuracy of at least 10^{-11}.

The minimization of $\Omega(\rho_{\mathbf{n}}, \mathbf{b}_i)$, which – in view of the specific numerical parameters mentioned above – was carried out in a parameter space of $\sim$ 512 000 dimensions was performed via a preconditioned conjugate gradient algorithm with adaptive step-size, as laid out in [16]. This can be considered as a refinement of the basic steepest

descent algorithm (see, for instance [38]). Within this algorithm, the gradients were calculated via analytic expressions. This procedure has proved rather robust, but in future developments other algorithms could be adopted, such as the limited-memory inverse Broyden method [17, 18], which would likely prove to be significantly more efficient.

As all the numerical calculations were rather time-consuming, use of shared memory parallelization via OpenMP was imperative. The calculations were carried out at the Vienna Scientific Cluster [39].

2.3. Analysis of the single-particle density profile

In order to analyze the single-particle density profile $\rho(\mathbf{r})$ on a quantitative level we introduce (i) its radius of gyration, R_{g}, and (ii) its radius of gyration tensor, $\mathcal{S}$, i.e., quantities which are often used to characterize the size and the shape of colloidal particles with complex internal shape. Based on the related, conventional definition of these quantities (see, for example, [40, 41]), we have generalized these expressions to our particular case.

We define the radius of gyration, R_{g}, and the position of the center of mass, $\mathbf{R}_{\mathrm{cm}}$, for our continuous single-particle density profile $\rho(\mathbf{r})$ via

$$R_{\mathrm{g}}^2 = \frac{1}{\mathcal{N}} \int_{\mathcal{C}} d\mathbf{r}\ \rho(\mathbf{r})(\mathbf{r} - \mathbf{R}_{\mathrm{cm}})^2 \quad \text{with} \quad \mathbf{R}_{\mathrm{cm}} = \frac{1}{\mathcal{N}} \int_{\mathcal{C}} d\mathbf{r}\ \rho(\mathbf{r})\mathbf{r} \tag{21}$$

and

$$\mathcal{N} = \int_{\mathcal{C}} d\mathbf{r}\ \rho(\mathbf{r}). \tag{22}$$

The shape of the single-particle density profile can most readily be characterized via the radius of gyration tensor (RGT) $\mathcal{S}$ [40, 41], whose elements S_{ij}, $i, j = 1, 2, 3$, have been evaluated for our particular case via

$$\mathcal{S}_{ij} = \frac{1}{\mathcal{N}} \int_{\mathcal{C}} d\mathbf{r}\ \rho(\mathbf{r})(r_i - R_{\mathrm{cm},i})(r_j - R_{\mathrm{cm},j}) \quad . \tag{23}$$

By definition, $\mathcal{S}$ is symmetric and real. One can easily verify, that $R_{\mathrm{g}}^2 = \mathcal{S}_{11} + \mathcal{S}_{22} + \mathcal{S}_{33} = \mathrm{Tr}(\mathcal{S})$. $\mathcal{S}$ can be diagonalized, with the real eigenvalues E_1, E_2, and E_3; without loss of generality it is assumed that $E_1 \geq E_2 \geq E_3$. The corresponding eigenvectors, which are mutually orthogonal, are denoted by $\mathbf{e}_i$.

Characterizing the single-particle density profile $\rho(\mathbf{r})$ by the eigenvalues of the RGT corresponds to approximating $\rho(\mathbf{r})$ by an ellipsoid of revolution centered at $\mathbf{R}_{\mathrm{cm}}$: the eigenvectors point along the principal axes and the square roots of the eigenvalues, i.e., $\sqrt{E_i}$, set the lengths of the three (orthogonal) semi-axes of the ellipsoid [26].

Based on the E_i, two further quantities which characterize the shape of the density profile can be calculated: (i) the asphericity parameter δ (as defined in [42]), and the acylindricity parameter ζ (as defined in [26] and references therein):

$$\delta = 1 - 3\frac{E_1E_2 + E_1E_3 + E_2E_3}{(E_1 + E_2 + E_3)^2} \quad (24)$$

$$\zeta = E_2 - E_3 \quad (\geq 0). \quad (25)$$

δ ranges from 0 (for spherical symmetry) to 1 (for a rod-like shape). In case $\zeta = 0$ (i.e. if $E_2 = E_3$) we have characterized the shape of the density profile via its aspect ratio $\sqrt{E_1/E_2}$.

3. Results

In the following we present and discuss data that we have obtained for the particle density profile $\rho(\mathbf{r})$. We remark that from here onwards we shall drop the specification "single" of the density profile, since – as will be discussed below – also aspherical GEM-4 particles show the phenomenon of multi-occupancy of the underlying lattice. In order to understand the impact of asphericity of the potential on the density profile, we have systematically varied the relevant parameters, i.e., the aspect ratio λ – see Subsec. 3.1 and the chemical potential (and hence the density) – see Subsec. 3.2.

For convenience we introduce the dimensionless temperature $T^* = k_\mathrm{B}T/\varepsilon$ and the reduced, dimensionless density $\rho^* = \sigma_0^3 \int d^3\mathbf{r}\rho(\mathbf{r})/V$. We further introduce – similar as in [16] – the density $\bar{\rho}$, defined as

$$\mu_\mathrm{ex} = \bar{\rho} \int d\mathbf{r}\Phi(\mathbf{r}), \quad (26)$$

where μ_ex is the excess chemical potential with respect to the ideal gas.

As mentioned above, also the disordered liquid phase can be captured within the present DFT formalism: this phase is characterized by a spatially constant density profile. Indeed, by fixing the temperature and increasing systematically the chemical potential, we are able to obtain the free energy F as a function of the density along a specific isotherm for the fluid phase and for the competing ordered phases. In principle, this information allows us to construct – e.g., via a common tangent construction – the coexistence densities of the competing phases. However, in the following we refrain from a discussion of the liquid phase and focus instead on the ordered phases and the respective density profiles.

3.1. Impact of the asphericity in the potential on the shape of the density profile

In order to study the impact of the asphericity in the interparticle interaction on the shape of the density profile $\rho(\mathbf{r})$, we have made a series of runs where we have – starting from the spherical case $\lambda = 1$ – gradually increased λ up to a value of 1.5. To this end we have fixed $T^* = 1.0$ and have considered two different densities, namely, $\bar{\rho}^* = 5.5$ and $\bar{\rho}^* = 7$.

Starting with the bcc equilibrium structure for the spherical case $\lambda = 1$ [16, 23, 27], we have increased λ in small steps, using the results for the equilibrium structure

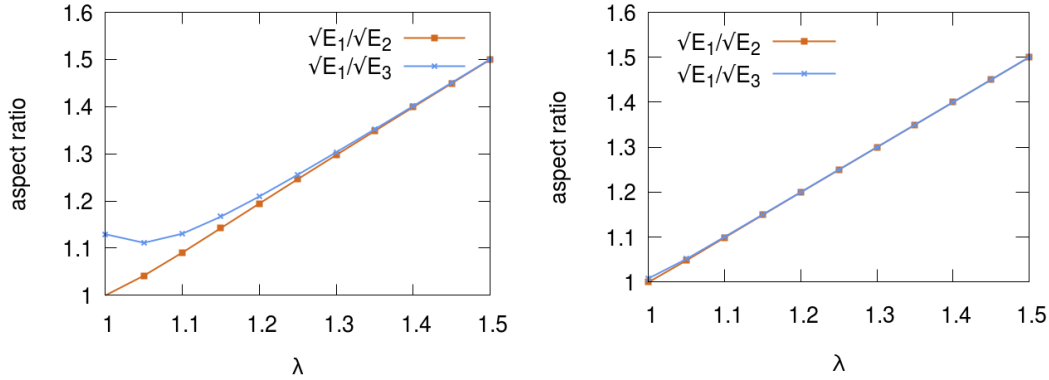

Figure 5. (color online) Variation of the aspect ratios of the density profile, $\sqrt{E_1/E_2}$ and $\sqrt{E_1/E_3}$ (as labeled), as obtained in our DFT calculations as the aspect ratio of the potential λ is varied. Left panel: $T^* = 1.0, \bar{\rho}^* = 5.5$, right panel: $T^* = 1.0, \bar{\rho}^* = 7.0$.

and for the density profile of the preceding λ-value as an input for the unconstrained minimization of the functional $\Omega[\rho]$ for the current λ-value.

Along this λ-variation we observe in the high density case $\bar{\rho}^* = 7$ that the shape of the interaction potential is essentially mirrored in the shape of the density profile: $\rho(\mathbf{r})$ has also shape of an ellipsoid of revolution (i.e., $E_2 = E_3$) and we find throughout that $\sqrt{E_1/E_2} \simeq \lambda$ (see Fig. 5). This behaviour is not very surprising, if we consider the occupancy number n_c of these multiply occupied lattices (see Fig. 7 and the related discussion below). Already for moderate densities, n_c attains values around six, meaning that the particles populating a specific lattice site experience a strong repulsion from the particles located on the neighbouring lattice sites. The natural consequence is that the particles of a specific site arrange into a spatial shape that reflects the geometry of the underlying potential; some further remarks to this issue are summarized in the discussion of Fig. 11. Furthermore, our results provide evidence that, as soon as λ starts to grow from the value 1, the eigenvector $\mathbf{e}_1$ of the RGT $\mathcal{S}$ given by Equation (23), which corresponds to the largest eigenvalue of $\mathcal{S}$, aligns with $\mathbf{n}$, i.e., the orientation of the main axis of $\Phi(\mathbf{r})$ (not shown; for details see [43]). Of course, the other eigenvectors, $\mathbf{e}_2$ and $\mathbf{e}_3$, span the plane orthogonal to $\mathbf{n}$. Moreover, increasing λ also imposes an increasingly strong deformation of the unit cell. This distortion can easily be quantified via the angles enclosed by the lattice vectors $\mathbf{a}_i$: the cell becomes increasingly skewed as λ increases; for an example see Fig. 6.

At the smaller density, i.e., $\bar{\rho}^* = 5.5$, the situation is at least for $\lambda \lesssim 1.25$ markedly different: while $\sqrt{E_1/E_2} \equiv \lambda$ over the considered λ-range, the values of $\sqrt{E_1/E_3}$ do differ from the respective λ: thus, in this λ-regime the density profile can no longer be approximated by an ellipsoid of revolution. However, with increasing λ, the density profile assumes within high numerical accuracy the shape of ellipsoid of revolution, whose aspect ratio is imposed by the respective value of λ for reasons similar to the ones put forward for the high density case.

Our results thus provide evidence that both for a high value of the density and a relatively strong asphericity the density profiles originating from our aspherical potential can be locally approximated very well by an ellipsoid of revolution which is oriented along the main axis of the potential $\mathbf{n}$, and whose shape reflects the shape of the interaction. Only for relatively small densities and up to intermediate values of the aspect ratio λ, deviations from this shape can be observed in the density profile.

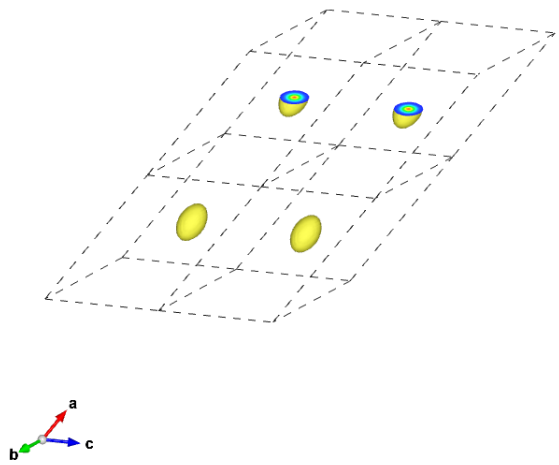

Figure 6. (color online) A representation of the density profile $\rho^*(\mathbf{r})$ for $\lambda = 1.5$ and $T^* = 0.5$, $\rho^* = 8.32$, showing four replicas of the primitive cell. The lengths of the cell axes are $a = 2.09$, $b = 1.60$, $c = 1.49$ in units of σ_0. The isosurfaces at which $\rho^*(\mathbf{r}) = 60$, corresponding to $\sim 1\%$ of the peak value, have been displayed in yellow. The upper cells show a section of $\rho^*(\mathbf{r})$ inside the domain bounded by the isosurfaces.

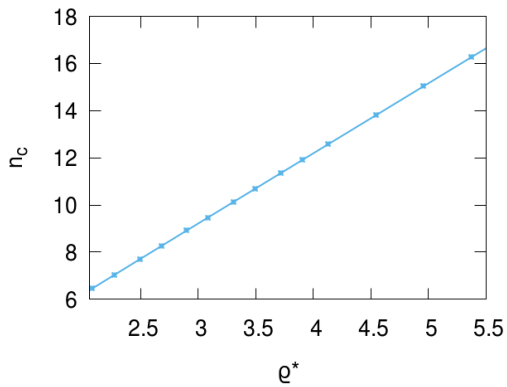

Figure 7. (color online) Occupation number n_c as a function of the density ρ^*. Here $T^* = 0.5$ and $\lambda = 1.5$.

3.2. Variation of the density profile with the chemical potential

To describe the dependence of the density profile $\rho(\mathbf{r})$ on the average density, we have systematically increased the chemical potential μ, keeping the temperature fixed at $T^* = 0.5$ and setting $\lambda = 1.5$. We have carefully checked that within the considered range of μ the ordered phase is more stable than the disordered, liquid phase, i.e., has the lower grand potential. Similarly to the spherically symmetric case, the ultrasoft interaction at hand leads to cluster crystals, whereby each lattice site is multiply occupied, and the lattice site occupation number n_c shows a linear dependence on the density ρ^*, as displayed in Fig. 7. This behavior is characteristic of the crystal phases of so-called $Q^{\pm}$ potentials, and is due to the fact that their lattice constants, unlike those of atomic crystals, are nearly state-independent [23, 30].

In the two panels of Fig. 8 data for the free energy F (in dimensionless, reduced units), and the volume of the unit cell of the underlying lattice, v, are shown as functions of the reduced density ρ^*. As expected, F increases with increasing ρ^*,

whereas v monotonously decreases with ρ^*, but very weakly so, consistently with the above-mentioned behavior of the lattice constants.

We now proceed to a quantitative analysis of the density profile in the neighborhood of a given lattice site, starting with the radius of gyration, $R_{\rm g}$ (Fig. 9), and the asphericity δ and the acylindricity ζ parameters (both in Fig. 10). $R_{\rm g}$ decays monotonically with increasing ρ^*, as expected for ultrasoft potentials. This rapid, non-linear decay with the density is again imposed by the increasing number of particles that populate the neighbouring lattice sites, leading thus to an increase in the repulsion that the particles of a specific lattice site experience: as a consequence, the density profile shrinks in size. The δ-values converge rather fast with increasing density towards a value of $\delta \simeq 0.087$, corresponding to a moderate deviation from sphericity. The increase in δ by about 10% over the observed density range is moderate and reflects on a quantitative level that the density profile assumes an ellipsoidal shape. Also the acylindricity parameter ζ is characterized by rather small values (i.e., throughout smaller than 0.05) and vanishes for $\rho^* \gtrsim 3.3$.

The aspect ratio of the density profile, expressed via $\sqrt{E_1/E_2}$ shown in Fig. 11, differs at intermediate densities from the value of the aspect ratio of the interaction, i.e., $\lambda = 1.5$; in this density regime the density profile is not an ellipsoid of revolution. This observation is nicely compatible with the above discussion of the λ dependence of the shape of the density profile (see Subsec. 3.1): at the lowest densities investigated, the occupancy number at a given lattice site is still small enough; therefore the particles are not able to exert a substantial repulsion on the particles of a neighbouring lattice site, which can therefore deviate in their density profile from the elliptic shape. However, already for $\rho^* \simeq 3$, the ratio $\sqrt{E_1/E_2}$ (and also $\sqrt{E_1/E_3}$, which is not shown) attains the value of 1.5; as shown in Fig. 10, the density profile has now rotational symmetry around its main axis. This limiting behaviour at high densities is reminiscent of the alignment of the density profile parallel to the main axis of the potential as reported in Subsection 3.1. Finally, we note that at intermediate densities the main axis of the density profile is not necessarily oriented parallel to the direction of the main axis of the interaction: both $\mathbf{e}_2 \cdot \mathbf{n}$ and $\mathbf{e}_3 \cdot \mathbf{n}$, as well as $\mathbf{e}_1 \cdot \mathbf{n}$ differ from their respective values for perfect alignment (i.e., 0 and 1, respectively) by less than 10 % (see panels of Fig. 12). Further increasing the density forces the density profile to align in the direction of the main axis of the potential.

Summarizing, results shown in Figs. 10, 11, and 12 indicate that the parameters that specify the shape and the orientation of the density profiles assume for $\rho^* \gtrsim 3$ essentially density-independent values.

4. Conclusions

In this contribution we have studied the local structure of the density profiles of ultrasoft, aspherical particles via classical density-functional theory. For the interaction of the particles we have assumed an aspherical version of the ultrasoft generalized exponential model of index n with $n = 4$, where asphericity is introduced via an intrinsic length scale parameter, which now depends on the center-to-center vector between two interacting particles and their orientations in space; the particles are thus modelled as (prolate) ellipsoids of revolution, with an aspect ratio $\lambda > 1$. For simplicity we have further assumed that particles located on different lattice sites have parallel orientation. For the excess free energy functional we have used a mean-field format. Optimization of the grand-potential functional has been performed with respect to the

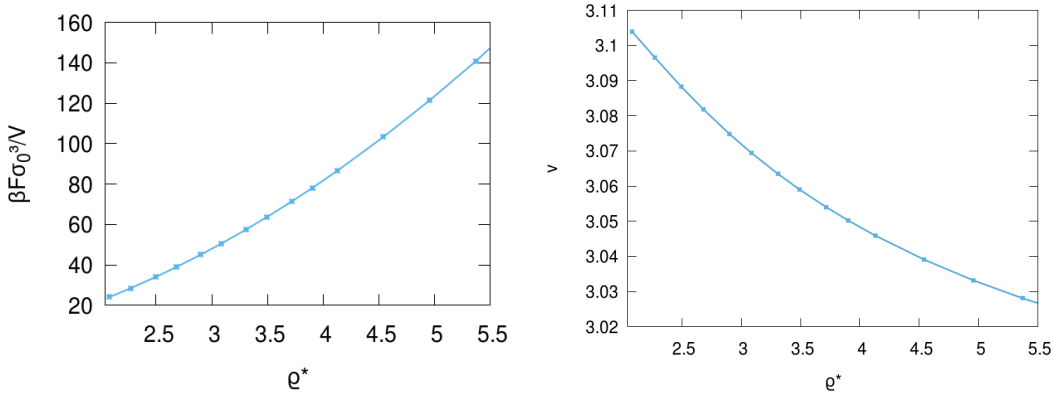

Figure 8. (color online) Left panel: free energy, F, in reduced dimensionless units (as specified) as a function of ρ^* (for $T^* = 0.5$ and $\lambda = 1.5$). Right panel: the same for the volume of the lattice unit cell, v (in units σ_0^3).

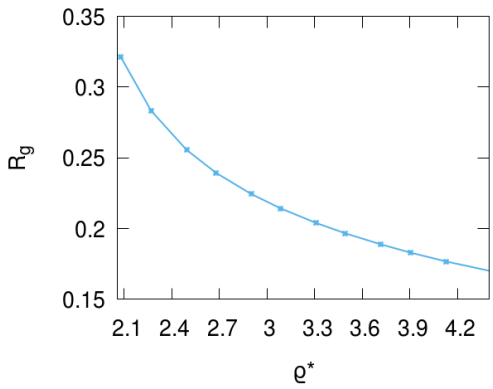

Figure 9. (color online) Radius of gyration, R_g (in units of σ_0), as a function of ρ^* (for $T^* = 0.5$ and $\lambda = 1.5$).

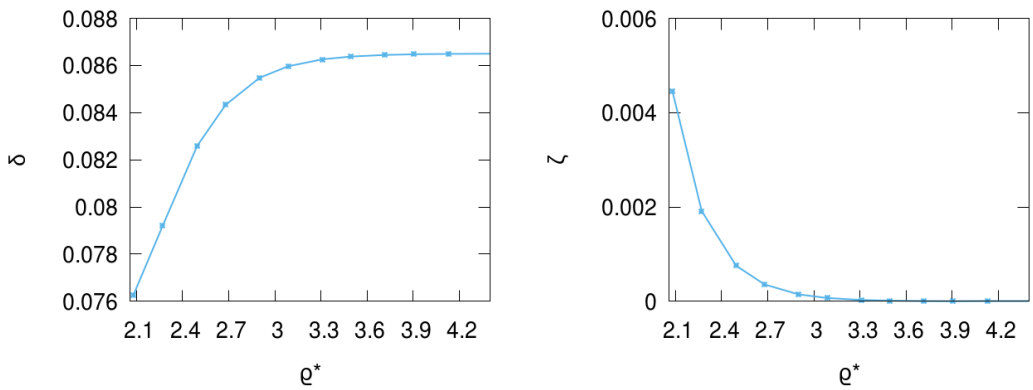

Figure 10. (color online) Asphericity, δ, and acylindricity, ζ, as defined in Equations (24), (25) as functions of ρ^* (for $T^* = 0.5$ and $\lambda = 1.5$).

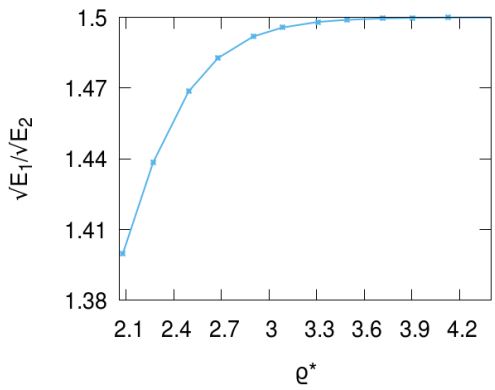

Figure 11. (color online) Aspect ratio of the density profile, expressed via $\sqrt{E_1/E_2}$, as a function of ρ^* (for $T^* = 0.5$ and $\lambda = 1.5$).

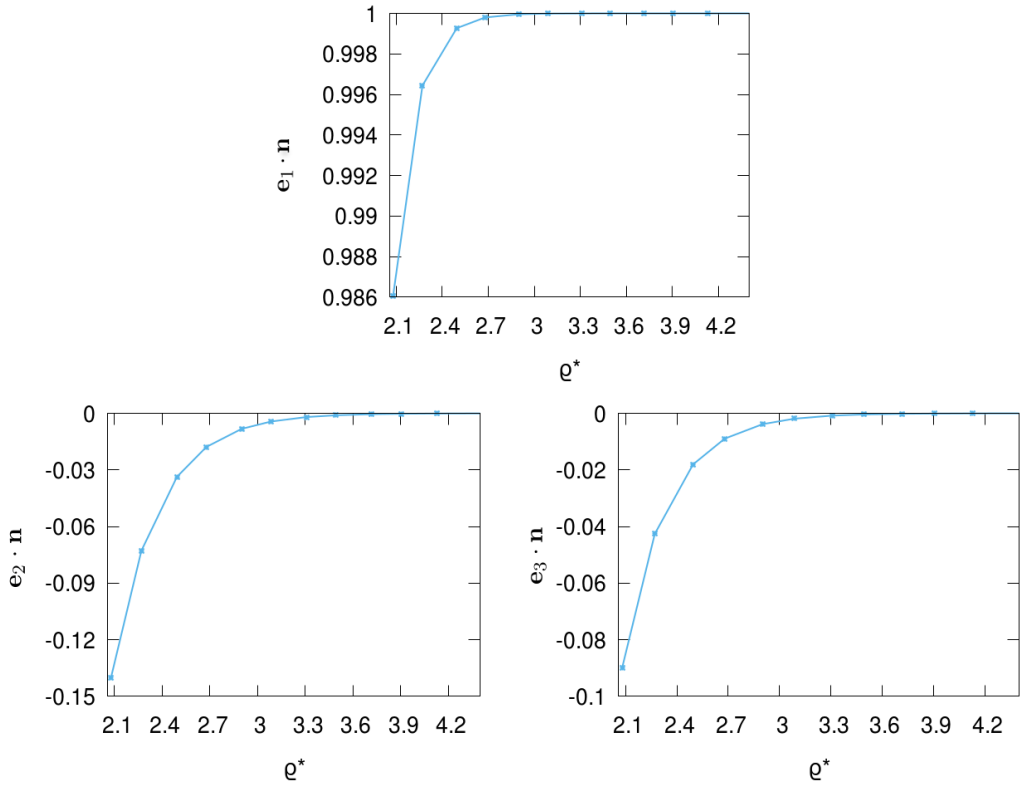

Figure 12. (color online) Orientation of the main axes of the density profile, $\mathbf{e}_1$, $\mathbf{e}_2$, and $\mathbf{e}_3$, with respect to the orientation of the main axis of the interaction potential, $\mathbf{n}$, expressed via $\mathbf{e}_1 \cdot \mathbf{n}$, $\mathbf{e}_2 \cdot \mathbf{n}$, and $\mathbf{e}_3 \cdot \mathbf{n}$, as functions of ρ^* (for $T^* = 0.5$ and $\lambda = 1.5$).

lattice vectors as well as to the density profile, which has been discretized on 80^3 grid points in the lattice unit cell, and has been carried out in a free, i.e., unbiased manner.

Varying the temperature, the chemical potential (and thus the density), and the aspect ratio λ we have investigated the impact of these parameters on the shape of the density profile $\rho(\mathbf{r})$. Variation of λ keeping the other parameters fixed forces the orientation of the density profile to align with the main axis of the interparticle interaction, leading also to an increasingly strong distortion of the underlying lattice as λ increases; in addition, $\rho(\mathbf{r})$ assumes the same value of aspect ratio as the interaction. An increase of the chemical potential leads at higher densities to an ellipsoidal shape of the density profile, which mirrors on a quantitative level the shape and the orientation of the underlying interparticle potential. Only at intermediate densities, relatively small deviations from this behaviour can be observed.

Some of the interesting physics that can emerge from this formalism will be postponed to future investigations and publications. Assuming a multi-component system, one might study the case where the density profiles located on different lattice sites are no longer identical, but can show different shapes and orientations. Along a different line, one could investigate if the predicted density profiles are faithful, i.e., if they describe in a quantitative manner the related density profiles as predicted in computer simulations on a monomeric level, where these "effective particles" on which the current investigations are based, are represented on a monomeric, atomistic level.

Acknowledgements

M.W. and G.K. gratefully acknowledge financial support by the Austrian Science Foundation (FWF) under projects Nos. P23910-N16 and F41 (SFB ViCoM) and by E-CAM, an e-infrastructure center of excellence for software, training and consultancy in simulation and modelling funded by the EU (Proj. No. 676531). W.M. and G.K. further acknowledge fruitful discussions with Roland Roth (Tübingen). M.W. acknowledges the kind hospitality at the Dipartimento di Fisica in Milano, where part of the work was carried out. D.P. acknowledges financial support from the TU Wien during his visit at TU Wien.

It is a particular pleasure to perform research in the same community as Daan Frenkel. The authors express their gratitude to Daan for so many enriching, enlightening, and joyful talks and discussions and for demonstrating that research can be so enjoyable.

References

[1] A. Donev, I. Cisse, D. Sachs, E.A. Variano, F.H. Stillinger, R. Connelly, S. Torquato, and P.M. Chaikin, Science **303**, 990 (2004).
[2] B.S. John, C. Juhlin, and F.A. Escobedo, J. Chem. Phys. **128**, 044909 (2008).
[3] A. Haji-Akbari, M. Engel, A.S. Keys, X.Y. Zheng, R.G. Petschek, P. Palffy-Muhoray, and S.C. Glotzer, Nature **462**, 773 (2009).
[4] U. Agarwal and F. A. Escobedo, Nat. Mater. **10**, 230 (2011).
[5] L. Rossi, S. Sacanna, W.T.M. Irvine, P.M. Chaikin, D.J. Pine, and A.P. Philipse, Soft Matter **7**, 4139 (2011).
[6] P. F. Damasceno, M. Engel, and S. C. Glotzer, Science **337**, 453 (2012).
[7] E. Bianchi, R. Blaak, and C.N. Likos, Phys. Chem. Chem. Phys **13**, 6397 (2011).

[8] E. Bianchi, G. Kahl, C.N. Likos, and F. Sciortino, J. Phys. (Condens. Matter) **27**, 230301 (2015).
[9] E. Bianchi, P.D.J. van Oostrum, C.N. Likos, and G. Kahl, Curr. Opin. Coll. Int. Science **30**, 18 (2017).
[10] E. Bianchi, B. Capone, I. Coluzza, L. Rovigatti, and P.D.J. van Oostrum, Phys. Chem. Chem. Phys. **19**, 19847 (2017).
[11] D. Frenkel and B. Smit, *Understanding Molecular Simulations* (Academic Press, San Diego, 2002).
[12] M.P. Allen and D. Tildesley, *Computer Simulations of Liquids* (Oxford, Oxford, 2017).
[13] R. Evans, Adv. Phys. **28**, 143 (1979).
[14] R. Evans, *Fundamentals of Inhomogeneous Fluids* (ed.: D. Henderson) (New York: Dekker) Chapter 3 (1992).
[15] R. Evans, M. Oettel, R. Roth, and G. Kahl, J. Phys. (Condens. Matter) **28**, 240401 (2016) and references in this Special Issue.
[16] D. Pini, A. Parola, and L. Reatto, J. Chem. Phys. **143**, 034902 (2015).
[17] M. Edelmann and R. Roth, Phys. Rev. E **93**, 062146 (2016).
[18] M. Edelmann and R. Roth, J. Chem. Phys. **144**, 074105 (2016).
[19] D. Stopper and R. Roth, J. Chem. Phys. **147**, 064508 (2017).
[20] D. Pini and A. Parola, Soft Matter **13**, 9259 (2017).
[21] A.A. Louis, P.G. Bolhuis, J.-P. Hansen, and E.J. Meijer, Phys. Rev. Lett. **85**, 2522 (2000).
[22] B.M. Mladek, G. Kahl, and C.N. Likos, Phys. Rev. Lett. **100**, 028301 (2008).
[23] B.M. Mladek, D. Gottwald, G. Kahl, M. Neumann, and C.N. Likos, Phys. Rev. Lett. **96**, 045701 (2006); *ibid.* **97** 019901 (2006).
[24] P.K. Maiti, G. Wang and W.A. Goddard, Macromolecules **37**, 6236 (2004).
[25] I.A. Georgiou, PhD Thesis (TU Wien, 2014) `http://smt.tuwien.ac.at/publications/theses.htm`.
[26] I.A. Georgiou, P. Ziherl, and G. Kahl, EPL **106**, 44004 (2014).
[27] B.M. Mladek, D. Gottwald, G. Kahl, C.N. Likos, and M. Neumann, J. Phys. Chem. B **111**, 12799 (2007).
[28] J.G. Gay and B.J. Berne, J. Chem. Phys. **74**, 3316 (1981).
[29] A. Ghoufi, D. Morineau, R. Lefort, and P. Malfreyt, J. Chem. Phys. **134**, 034116 (2011).
[30] C.N. Likos, B.M. Mladek, D. Gottwald, and G. Kahl, J. Chem. Phys. **126**, 224502 (2007).
[31] C.N. Likos, B.M. Mladek, A.J. Moreno, D. Gottwald, and G. Kahl, Comp. Phys. Commun. **179**, 71 (2008).
[32] B.M. Mladek, P. Charbonneau, C.N. Likos, D. Frenkel, and G. Kahl, J. Phys. (Condens. Matter) **20**, 494245 (2008).
[33] C.N. Likos, A. Lang, M. Watzlawek, and H. Löwen, Phys. Rev. E **63**, 031206 (2001).
[34] S. Prestipino and F. Saija, J. Chem. Phys. **126**, 194902 (2007).
[35] A. Nikoubashman and C.N. Likos, J. Phys. (Condens. Matter) **22**, 104107 (2010).
[36] See, for instance, J.-P. Hansen and I.R. McDonald, *Theory of Simple Liquids*, Academic Press, London, 2013.
[37] M. Frigo and S.G. Johnson, Proceedings of the IEEE **93**, 216 (2005).
[38] W.H. Press, S.A. Teukolsky, W.T. Vetterling, and B.P. Flannery, *Numerical Recipes, 3rd ed.* (Cambridge University Press, 2007).
[39] www.vsc.ac.at.
[40] K. Šolc and W.H. Stockmayer, J. Chem. Phys. **54**, 2756 (1971).
[41] K. Šolc, J. Chem. Phys. **55**, 335 (1971).
[42] J. Rudnick and G. Gaspari, J. Phys. A (Math. General) **19**, L191 (1986).
[43] M. Weißenhofer, Master Thesis (TU Wien, 2017) `http://smt.tuwien.ac.at/publications/theses.htm`.